



HAL
open science

Three-dimensional structure of the Upper Scorpius association with the Gaia first data release

Phillip A. B. Galli, Isabelle Joncour, Estelle Moraux

► **To cite this version:**

Phillip A. B. Galli, Isabelle Joncour, Estelle Moraux. Three-dimensional structure of the Upper Scorpius association with the Gaia first data release. *Monthly Notices of the Royal Astronomical Society: Letters*, 2018, 477, pp.L50-L54. 10.1093/mnrasl/sly036 . insu-03693551

HAL Id: insu-03693551

<https://insu.hal.science/insu-03693551>

Submitted on 13 Jun 2022

HAL is a multi-disciplinary open access archive for the deposit and dissemination of scientific research documents, whether they are published or not. The documents may come from teaching and research institutions in France or abroad, or from public or private research centers.

L'archive ouverte pluridisciplinaire **HAL**, est destinée au dépôt et à la diffusion de documents scientifiques de niveau recherche, publiés ou non, émanant des établissements d'enseignement et de recherche français ou étrangers, des laboratoires publics ou privés.

Three-dimensional structure of the Upper Scorpius association with the *Gaia* first data release

Phillip A. B. Galli,¹★ Isabelle Joncour^{2,3}★ and Estelle Moraux²★

¹*Instituto de Astronomia, Geofísica e Ciências Atmosféricas, Universidade de São Paulo, Rua do Matão 1226, Cidade Universitária, 05508-900 São Paulo – SP, Brazil*

²*Université Grenoble Alpes, CNRS, IPAG, F-38000 Grenoble, France*

³*Department of Astronomy, University of Maryland, College Park, MD 20742, USA*

Accepted 2018 March 2. Received 2018 March 2; in original form 2017 November 21

ABSTRACT

Using new proper motion data from recently published catalogues, we revisit the membership of previously identified members of the Upper Scorpius association. We confirmed 750 of them as cluster members based on the convergent point method, compute their kinematic parallaxes, and combined them with *Gaia* parallaxes to investigate the 3D structure and geometry of the association using a robust covariance method. We find a mean distance of $146 \pm 3 \pm 6$ pc and show that the morphology of the association defined by the brightest (and most massive) stars yields a prolate ellipsoid with dimensions of $74 \times 38 \times 32$ pc³, while the faintest cluster members define a more elongated structure with dimensions of $98 \times 24 \times 18$ pc³. We suggest that the different properties of both populations are an imprint of the star formation history in this region.

Key words: methods: statistical – proper motions – stars: distances – Galaxy: kinematics and dynamics – open clusters and associations: individual: Upper Scorpius.

1 INTRODUCTION

The Upper Scorpius association, located at a distance of about 145 pc, is the youngest (~ 5 – 10 Myr; Preibisch et al. 2002; Pecaut & Mamajek 2016) and best studied subgroup of the Scorpius–Centaurus complex. Despite its close proximity to the Ophiuchus star-forming clouds, there are no indications of ongoing star formation activity. The molecular clouds in this region have already been dispersed so that cluster members of different masses are still present and can be easily observed. de Zeeuw et al. (1999) investigated the high-mass stellar population of the association ($M \geq 2 M_{\odot}$) and identified most of the group members with spectral types B, A, and F. Later studies focused on the low-mass content of the association, identifying hundreds of late-type stars and brown dwarfs (see e.g. Preibisch & Zinnecker 1999; Preibisch et al. 2002; Luhman & Mamajek 2012; Lodieu 2013; Rizzuto, Ireland & Kraus 2015; Cook, Scholz & Jayawardhana 2017).

The age estimate of Upper Scorpius is controversial. While previous works reported an age of ~ 5 Myr with very little spread (Preibisch & Zinnecker 1999; Preibisch et al. 2002; Slesnick, Hillenbrand & Carpenter 2008), more recent studies indicate an older median age (10–11 Myr) with a spread as large as ~ 7 Myr (Pecaut, Mamajek & Bubar 2012), with a possible dependence on position (Pecaut & Mamajek 2016), effective temperatures (Rizzuto et al. 2016), or the presence of circumstellar disc (Donaldson et al.

2017). Whether this age spread is real or not (see e.g. Fang, Herczeg & Rizzuto 2017) remains under debate.

In this context, another important aspect is the intrinsic size of the association and the spread of individual distances, which causes the stellar luminosities (and ages) to be over- or underestimated with respect to the mean distance of the association. de Zeeuw et al. (1999) derived a mean distance of 145 ± 2 pc based on trigonometric parallaxes from the *Hipparcos* catalogue (ESA 1997) of 120 bright cluster members. The spread of distances for this sample amounts to about 32 pc, which is consistent with the projected diameter of the association of $\sim 14^{\circ}$ that roughly corresponds to 35 pc. Thus, based on these data, we may assume that the bright stars' spatial distribution has a spherical shape (see also Preibisch & Mamajek 2008). Recent studies led by Fang et al. (2017) and Cook et al. (2017) estimated a mean distance of 144 and 145 ± 2 pc, and a spread along the line of sight of about ± 15 and ± 13 pc, respectively. However, a complete study of the 3D geometry of the Upper Scorpius association and its dependence with stellar masses is still lacking. This situation will improve dramatically in the near future with the trigonometric parallaxes delivered by the *Gaia* satellite down to $G \simeq 20$ mag. In this Letter, we use the first data release of the *Gaia* satellite (*Gaia*-DR1) together with the more recent ground-based surveys to investigate the 3D structure and membership of the association.

2 SAMPLE OF UPPER SCORPIUS STARS

The first step in our analysis is to build a complete census of known members in the Upper Scorpius association. We have compiled

* E-mail: phillip.galli@iag.usp.br (PABG); isabelle.joncour@univ-grenoble-alpes.fr (IJ); estelle.moraux@univ-grenoble-alpes.fr (EM)

a list of 1322 stars that were identified in previous studies to be likely members of the association based on youth diagnostics and proper motions (de Zeeuw et al. 1999; Preibisch & Zinnecker 1999; Preibisch et al. 2002; Rizzuto, Ireland & Robertson 2011; Luhman & Mamajek 2012; Rizzuto, Ireland & Kraus 2015; Pecaut & Mamajek 2016). In the following, we searched the current data bases to access the more recent data available for this sample that will be useful to investigate the structure of the association.

The Tycho-*Gaia* Astrometric Solution (TGAS; Lindegren et al. 2016) that has just been delivered by *Gaia*-DR1 provides trigonometric parallaxes and proper motions for only 149 stars. On the other hand, the recently published ‘Hot Stuff for One Year’ (HSOY; Altmann et al. 2017) and UCAC5 proper motion catalogues provide proper motion measurements for 1011 stars and 729 stars in our sample, respectively. Both catalogues combine the stellar positions from *Gaia*-DR1 with ground-based astrometry from the PPMXL (Roesser, Demleitner & Schilbach 2010) and UCAC4 (Zacharias et al. 2013) catalogues, and represent the best present-day compromise for this work between the number of sources in our sample and proper motion precision. In addition, we also complement these two sources of proper motions with data from the SPM4 (Girard et al. 2011) catalogue for 783 stars. We compared the proper motions of the stars in our sample given by the different catalogues and detected some outliers in UCAC5. Thus, we use the TGAS and HSOY catalogues as main sources of proper motions and complement them with proper motions from UCAC5 and SPM4. Doing so, we find proper motion data for 1104 stars of our initial sample.

We also searched the literature for radial velocity information using the data mining tools available at the CDS/SIMBAD data bases (Wenger et al. 2000). Our search for radial velocities is based on Barbier-Brossat & Figon (2000), Nordström et al. (2004), Gontcharov (2006), Torres et al. (2006), Kharchenko et al. (2007), White, Gabor & Hillenbrand (2007), Holmberg, Nordström & Andersen (2007), Chen et al. (2011), Dahm, Slesnick & White (2012), Song, Zuckerman & Bessell (2012), Kordopatis et al. (2013), Malo et al. (2014), and Mann et al. (2016). We found radial velocities for 146 stars.

Table 1 lists the data collected for the stars in our sample and the results obtained in the forthcoming analysis. It is available only in electronic form at the CDS.

3 KINEMATIC PARALLAXES AND MEMBERSHIP ANALYSIS

The small number of stars with measured trigonometric parallaxes (i.e. 11 per cent of the sample) and the scarcity of radial velocity measurements are the main limitations in this work to investigate the structure and kinematics of Upper Scorpius. In this context, individual parallaxes for comoving members of the association sharing the same space motion can be inferred from the moving-cluster method (de Bruijne 1999a; Galli et al. 2012). The so-derived kinematic parallaxes are not as precise and accurate as the trigonometric parallaxes from the TGAS catalogue, but they still provide useful information to complement the forthcoming analysis.

To begin with, we take the sample of 1104 stars with known proper motions and perform a 3σ clipping on the distribution of both proper motion components to remove obvious outliers. This step reduces the sample to 891 stars. Then, we apply the convergent point search method (CPSM) as described in section 2 of Galli et al. (2017). The method takes a distance estimate and velocity dispersion of the cluster as input parameters. We use the distance of 145 pc and velocity dispersion of $\sigma_v \simeq 1.5 \text{ km s}^{-1}$ derived by de

Table 1. Properties of the 1322 stars in the Upper Scorpius region. We provide for each star the 2MASS identifier, position, proper motion, radial velocity, kinematic and trigonometric parallax, spatial velocity, and membership status based on the CPSM (‘Y’=yes, ‘N’=no). The CTRL column (‘Y’=yes, ‘N’=no) indicates the stars included in our control sample. The full table is available online.

2MASS identifier	α (h:m:s)	δ ($^{\circ}$ ' ")	$\mu_{\alpha} \cos \delta$ (mas yr $^{-1}$)	μ_{δ} (mas yr $^{-1}$)	Ref.	V_r (km s $^{-1}$)	Ref.	π_{kin} (mas)	π_{trig} (mas)	U (km s $^{-1}$)	V (km s $^{-1}$)	W (km s $^{-1}$)	CPSM	CTRL
J15302162-2036481	15 30 21.63	-20 36 48.12	-19.630 ± 0.176	-23.430 ± 0.071	TGAS	-31.3 ± 0.3	1	7.97 ± 0.71	6.84 ± 0.39	-30.2 $^{+0.9}_{-0.9}$	-14.3 $^{+1.2}_{-1.6}$	-17.8 $^{+1.3}_{-1.4}$	Y	N
J15311722-3349115	15 31 17.23	-33 49 11.56	-17.764 ± 0.985	-25.071 ± 0.942	HSOY								N	N
J15315022-3252519	15 31 50.22	-32 52 51.92	-17.269 ± 0.035	-22.233 ± 0.020	TGAS			5.95 ± 0.78					N	N
J15321033-2158004	15 32 10.33	-21 58 00.48	-16.07 ± 1.99	-23.58 ± 1.88	SPM4			7.46 ± 0.82					Y	N
J15322013-3108337	15 32 20.14	-31 08 33.75	-18.845 ± 0.057	-22.491 ± 0.042	TGAS	-1.4 ± 0.3	1		7.75 ± 0.52	-6.3 $^{+0.6}_{-0.8}$	-16.6 $^{+1.1}_{-1.6}$	-4.0 $^{+1.3}_{-1.4}$	N	N
J15325521-1651101	15 32 55.21	-16 51 10.18				1.8 ± 1.1	2						N	N
J15330951-2429253	15 33 09.51	-24 29 25.39	-24.748 ± 0.111	-33.503 ± 0.055	TGAS	-3.6 ± 0.6	3		11.79 ± 1.00	-6.0 $^{+1.1}_{-1.2}$	-15.4 $^{+1.3}_{-2.1}$	-5.1 $^{+1.6}_{-1.8}$	N	N
J15350863-252397	15 35 08.64	-25 32 39.73											N	N
J15351610-2544030	15 35 16.10	-25 44 03.07	-18.428 ± 0.042	-23.482 ± 0.023	TGAS	-2.54 ± 0.60	4	7.62 ± 0.63	7.44 ± 0.62	-6.0 $^{+1.1}_{-1.3}$	-17.9 $^{+1.4}_{-2.2}$	-4.7 $^{+1.7}_{-1.9}$	Y	Y
J15354856-2958551	15 35 48.56	-29 58 55.18	-41.096 ± 2.370	-40.788 ± 2.369	HSOY								N	N

Radial velocity references. (1) Chen et al. (2011), (2) Kharchenko et al. (2007), (3) Gontcharov (2006), (4) Dahm et al. (2012), (5) Torres et al. (2006), (6) White et al. (2007), (7) Mann et al. (2016), and (8) Kordopatis et al. (2013).

Table 2. Spatial velocity of the Upper Scorpius association derived from our control sample of 40 stars with complete data. We provide for each velocity component the mean, standard error of the mean (SEM), median, mode, and standard deviation (SD).

	Mean \pm SEM (km s ⁻¹)	Median (km s ⁻¹)	Mode (km s ⁻¹)	SD (km s ⁻¹)
<i>U</i>	-5.0 ± 0.1	-4.9	-4.7	2.2
<i>V</i>	-16.6 ± 0.1	-16.9	-16.7	1.5
<i>W</i>	-6.8 ± 0.1	-6.6	-6.6	1.5
V_{space}	18.8 ± 0.1	18.8	18.8	1.6

Bruijne (1999b). The method is rather insensitive to small variations of these parameters. Doing so, the CPSM selects 750 stars that we consider to be confirmed members of the Upper Scorpius association (see Table 1). The corresponding convergent point solution is located at $(\alpha_{\text{cp}}, \delta_{\text{cp}}) = (95^{\circ}2, -42^{\circ}8) \pm (2^{\circ}2, 2^{\circ}5)$ with $\chi_{\text{red}}^2 = 0.94$ and correlation coefficient of $\rho = -0.99$.

We note that 103 stars among the confirmed moving group members have trigonometric parallaxes, but only 51 stars exhibit complete data (proper motion, radial velocity, and trigonometric parallax). We convert their trigonometric parallaxes into distances using an exponentially decreasing space density prior with length-scale $L = 1.35$ kpc as described by Astraatmadja & Bailer-Jones (2016), and use them to calculate the three-dimensional Galactic spatial velocities UVW from the procedure described by Johnson & Soderblom (1987). Then, we perform an iterative 3σ clipping in the distribution of the UVW spatial velocities, and we end up with 40 stars that define our control sample (see Table 1). We argue that these stars are secure members of the association based on (i) the membership analysis performed with the CPSM and (ii) their common space motion as derived directly from proper motions, radial velocities, and trigonometric parallaxes. We provide in Table 2 the spatial velocity of the Upper Scorpius association as derived from our control sample.

We calculate kinematic parallaxes for the 750 stars identified as moving group members in our analysis using the formalism described in section 2.1 of Galli et al. (2017). We decided to compute the kinematic parallaxes using equation 2 of Galli et al. (2017) that is written in terms of the spatial velocity of the cluster. Although this procedure applies to all stars in the sample (including binaries and cluster members without radial velocity measurements), the so-derived parallaxes are less accurate than the results obtained directly from equation 1 of Galli et al. (2017) based on the radial velocity of individual stars. To overcome this issue, we performed Monte Carlo simulations (with 1000 iterations) by resampling the input parameters (proper motion, spatial velocity of the cluster, and angular distance to the convergent point position) in equation 2 of Galli et al. (2017) from Gaussian distributions where mean and variance correspond to the observed parameters and their uncertainties. We report for each star in Table 1 the mean and standard deviation of the distribution of simulated kinematic parallaxes. The comparison with the trigonometric parallaxes in our control sample for the sample in common (40 stars) yields a mean difference of -0.02 mas (in the sense ‘trigonometric’ minus ‘kinematic’) and rms of 0.5 mas. The mean error of the kinematic parallaxes derived in this work is 0.8 mas while the mean error of the TGAS trigonometric parallaxes in our sample is 0.5 mas. The systematic errors of 0.3 mas in the TGAS trigonometric parallaxes reported by Lindegren et al. (2016) were added quadratically to the parallax uncertainties in our analysis. We conclude that both samples (trigonometric and

kinematic parallaxes) are consistent between themselves within their errors.

We obtain a mean parallax of $\pi = 7.06 \pm 0.03$ mas based on the kinematic parallaxes derived in this Letter for the 750 stars. This corresponds to a distance of $d = 142 \pm 1$ pc given a confidence interval of 95 per cent. In comparison, the mean parallaxes obtained from the control sample (40 stars) and all TGAS trigonometric parallaxes (103 stars) are, respectively, $\pi = 7.09 \pm 0.09 \pm 0.30$ mas and $6.86 \pm 0.07 \pm 0.30$ mas. They yield a distance estimate of $d = 141 \pm 4 \pm 6$ pc and $146 \pm 3 \pm 6$ pc. The second term in our uncertainties refers to the systematic errors of the trigonometric parallaxes in the TGAS catalogue (see e.g. Lindegren et al. 2016). We consider the latter distance estimate as our final result, because it is based on a more significant number of cluster members (with measured trigonometric parallaxes) and it will be confirmed in our forthcoming analysis (see Section 5).

4 3D STRUCTURE

To investigate the structure of the association, we use the stellar parallaxes derived above to calculate the three-dimensional position XYZ of the selected group members in our sample. This reference system has its origin at the Sun, where X points to the Galactic Centre, Y points in the direction of Galactic rotation, and Z points to the Galactic north pole to form a right-handed system.

To derive the main 3D global geometrical properties of the Upper Scorpius association, we use a multivariate statistical method based on estimators of the covariance matrix of the 3D spatial distribution. The idea is that the envelope of any 3D distribution of points may be approximated by a Gaussian ellipsoid distribution that is free to rotate around any axes. The centre of the ellipsoid is the centroid of the stars of the cluster, and the 3×3 covariance matrix of this distribution of points contains the structural information of its orientation and its major directions of scatter in the three dimensions. Indeed, the eigenvectors of the covariance matrix \mathbf{C} constitute an orthonormal system of maximal variance, i.e. it gives the three main axes along which the data vary the most. The eigenvalues λ_i of the covariance matrix are related to the dispersion of the data along those principal axes. The semi-axes a_i of the ellipsoid are then defined as

$$a_i = (\chi^2(\alpha, d) \lambda_i)^{1/2}, \quad (1)$$

where χ^2 is the chi-squared function, d is the dimension of the space in which the data are embedded (i.e. $d = 3$), and α the quantile that defines the proportion of data that are contained within the ellipsoid.

To derive the vector and the angle of the rotation operation that brings the XYZ coordinate system in the orthonormal system of the optimal ellipsoid, we use the following equation:

$$\mathbf{C} \cdot \mathbf{V} = \mathbf{V} \cdot \mathbf{\Gamma}, \quad (2)$$

where \mathbf{V} is the matrix whose columns are composed of the three eigenvectors ($\mathbf{u}_{x'} = \{\mathbf{V}_{i1}\}$, $\mathbf{u}_{y'} = \{\mathbf{V}_{i2}\}$, $\mathbf{u}_{z'} = \{\mathbf{V}_{i3}\}$; $i = 1, 2, 3$) of the covariance matrix \mathbf{C} , and $\mathbf{\Gamma}$ is a diagonal matrix composed of the corresponding ordered eigenvalues. The matrix \mathbf{V} represents the rotation transformation matrix and $\mathbf{\Gamma}^{1/2}$ the scale matrix such that we have

$$\mathbf{C} = \mathbf{V} \cdot \mathbf{\Gamma}^{1/2} \cdot \mathbf{\Gamma}^{1/2} \cdot \mathbf{V}^{-1}. \quad (3)$$

In other words, we define the linear transformation $\mathbf{T} = \mathbf{V} \cdot \mathbf{\Gamma}^{1/2}$, such that the covariance matrix is defined as $\mathbf{C} = \mathbf{T} \cdot {}^t\mathbf{T}$, where ${}^t\mathbf{T}$ is the transpose matrix of \mathbf{T} . Applying the covariance matrix on

Table 3. Geometrical properties of the Upper Scorpius association obtained in each experiment E_i . We provide the distance D_0 of the ellipsoid centroid to the Sun, their Galactic Cartesian coordinates (x_0, y_0, z_0) , the eigenvectors of the covariance matrix (i.e. the vectors \mathbf{u} of the principal axes of the ellipsoid, X', Y', Z'), the semi-axes (a_1, a_2, a_3) of the ellipsoids, inclination i of the first main principal axis with respect to the Galactic plane, and the corresponding uncertainties.

Exp.	D_0 (pc)	x_0, y_0, z_0 (pc)	$\mathbf{u}_{x'}$	$\mathbf{u}_{y'}$	$\mathbf{u}_{z'}$	a_1 (pc)	a_2 (pc)	a_3 (pc)	i ($^\circ$)
E_1	145 ± 1	134.4; -22.2; 49.8	0.897; -0.140; 0.418	-0.391; 0.185; 0.901	-0.203; -0.973; 0.111	37 ± 3	19 ± 1	16 ± 1	25 ± 3
E_2	144 ± 2	133.1; -21.7; 50.5	0.935; -0.022; 0.353	-0.351; 0.066; 0.934	-0.044; -0.998; 0.054	38 ± 3	18 ± 1	14 ± 1	20 ± 6
E_3	142 ± 3	130.4; -16.3; 54.9	0.904; -0.097; 0.417	0.063; 0.993; 0.095	-0.424; -0.060; 0.904	51 ± 4	10 ± 2	6 ± 1	25 ± 1
E_4	142 ± 3	131.3; -18.7; 51.6	0.912; -0.112; 0.395	-0.271; 0.561; 0.783	-0.309; -0.820; 0.481	48 ± 5	13 ± 1	10 ± 1	23 ± 2
E_5	142 ± 2	129.8; -16.5; 54.5	0.903; -0.096; 0.418	0.006; 0.977; 0.213	-0.429; -0.191; 0.883	52 ± 4	10 ± 1	6 ± 1	25 ± 1
E_6	142 ± 3	130.7; -18.3; 51.6	0.909; -0.113; 0.401	-0.264; 0.587; 0.765	-0.322; -0.801; 0.504	49 ± 5	12 ± 1	9 ± 1	24 ± 2

any set of white noise will transform the set of white data into the rotated and scaled data that fit the ellipsoid.

The inclination angle i of the most elongated principal axis of the ellipsoid (oriented along the vector $\mathbf{u}_{x'} = \{\mathbf{V}_{i1}\}$, $i = 1, 2, 3$) with respect to the Galactic plane is estimated from

$$i = \text{atan}(\mathbf{V}_{31}/(\mathbf{V}_{11}^2 + \mathbf{V}_{21}^2)^{1/2}). \quad (4)$$

In the standard covariance method, all data are taken into account to compute the covariance matrix \mathbf{C} , which is fine for a homogeneous distribution. But when the distribution of points is more complex, as for example a compact region with sparse and diffuse tails or the presence of noise and outliers (as in our data), a robust estimator of the covariance matrix is required. In order to define the main optimal properties of the ellipsoid (location, orientation, and scatter), we choose the minimum covariance determinant (MCD) estimator as it is the most robust in the presence of a high proportion of outliers (Rousseeuw & Driessen 1999; Rousseeuw & Hubert 2011), when compared for example to the *robust* minimum volume ellipsoid estimator (Van Aelst & Rousseeuw 2009). The MCD estimator searches for the ellipsoid with the smallest determinant that covers a specified ‘good’ fraction of the data. No less than half of the data have to be used. Since the data are not homogeneously distributed, the method may lead to local attractors if the fraction of data is inadequate. We found that taking 80 per cent as the minimum required fraction of data used in the MCD estimator allows us to get rid of the outliers and ensures the uniqueness and stability of the solution.

We then apply this method to three different subsamples of our list of 750 stars considered as cluster members from the CPSM (see the previous section): the TGAS stars only, corresponding to the brightest stars (S_1 , $n_1 = 103$ stars); all the stars of our catalogue having a kinematic parallax estimate (S_2 , $n_2 = 750$ stars); and finally the stars that have a kinematic parallax estimate but are not in TGAS (S_3 , $n_3 = 647$ stars). From those samples, we perform six calculations depending on whether we use the trigonometric or kinematic parallaxes to compute the 3D Galactic coordinates of the stars in sample S_1 (respectively experiments E_1 and E_2), and depending on the bootstrap technique we used for the samples S_2 and S_3 (experiments E_3 to E_6).

Indeed, in order to derive the geometrical properties in a statistical and robust way, we implement two different bootstrap iterative methods (5000 iterations). The first bootstrap technique (B_1) is based on a Monte Carlo sampling applied to the coordinates (right ascension, declination, and parallax), taking into account their normally distributed uncertainties to compute their Galactic coordinates. This bootstrap technique aims at evaluating the effect of the individual uncertainties of the star positions on the global structure of the association. The second bootstrap method (B_2) takes into account the fact that the sample sizes are different. When

comparing the distribution of the 103 brightest (and therefore most massive assuming that they are located approximately at the same distance) stars from sample S_1 to the 647 less bright (less massive) stars (sample S_3), we need to estimate the possible bias introduced by the different sample size. We thus realize a Monte Carlo sampling of 103 stars within the S_2 and S_3 samples, to which we apply the B_1 bootstrap method to compute the Galactic coordinates. For each of the experiments, we derive the mean centre, the lengths and direction of the main axes of the ellipsoid, and the inclination of the most elongated axis of the ellipsoid with respect to the Galactic plane (see Table 3). The 3D spatial study of the Upper Scorpius association has been performed in the *R environment* (R Core Team 2017) using the *MASS* package (Venables & Ripley 2002) for the MCD spatial analysis and the *RGL* (Adler et al. 2017) package for the 3D visualization.

5 DISCUSSION AND CONCLUSION

Despite the different data sets used in E_1 and E_2 (trigonometric and kinematic parallaxes), we confirmed that the global 3D distributions are similar. In both cases, the geometry of the S_1 sample is a prolate structure elongated mainly along the X -axis (oriented towards the Galactic Centre) with the E_1 dimensions $\sim 74 \times 38 \times 32 \text{ pc}^3$, and an inclination of $i = 20^\circ - 25^\circ$ with the Galactic plane. The computed centroids of the ellipsoids are about 1 pc away from each other and are located at a distance of 145 and 144 pc for E_1 and E_2 , respectively. The average value is consistent with our distance estimate of $146 \pm 3 \pm 6 \text{ pc}$ derived in Section 3 for this sample. We note that intriguingly the inclination i obtained in this work is very close to the one derived for the overall structure of the Gould belt (Perrot & Grenier 2003; Palouš & Ehlerová 2017).

We check that no bias is introduced by sample size effect in our analysis by using the two bootstrap techniques described earlier. E_3 and E_4 (resp. E_5 and E_6) experiments give the same results within the standard deviations. We compare the shape of the ellipsoids that we obtain for the stars present in the TGAS catalogue S_1 sample, corresponding in majority to the brightest ($G < 12 \text{ mag}$) and therefore most massive stars, to the fainter and less massive S_3 sample. The ellipsoid associated with the faintest stars (E_6 experiment) has a 3D dimension of $\sim 98 \times 24 \times 18 \text{ pc}^3$. The ratio of semi-axes between the ellipsoids E_2 and E_6 illustrated in Fig. 1 is 1.3, 0.7, and 0.6. These results may suggest that the formation of the more massive stars took place first, before the formation of the less massive stars, which would allow a slight relaxation for the most massive stars set. This would be seen as a less E_2 anisotropic structure compared to the very elongated E_6 ellipsoid and favour a real age spread.

The anisotropy of the shape of both ellipsoids suggests that the Upper Scorpius association is not dynamically relaxed. Indeed, using a one-dimensional velocity dispersion of 2.2 km s^{-1} for the

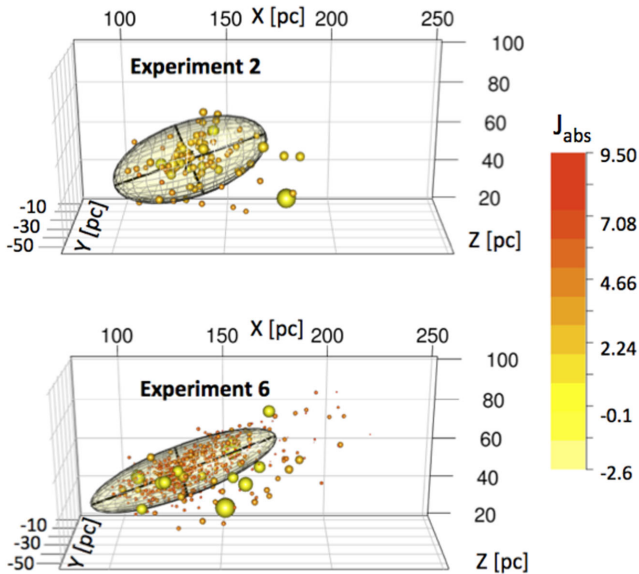


Figure 1. 3D structure of the Upper Scorpius association obtained for the experiments E_2 (upper panel) and E_6 (lower panel). The colour and size of the points are related to the absolute magnitude of the stars computed from the 2MASS J filter.

brightest star sample (see Table 2) and 11 Myr (Pecaut et al. 2012) as the estimated age of the region, the crossing distance is of the order of ~ 25 pc, which is less than the largest dimension of the ellipsoid. We thus conclude that the shape of the Upper Scorpius association is an imprint of its star formation history. This study represents an important step towards understanding the complex history of the star formation process in this region. The more accurate parallaxes from *Gaia*-DR2 for the faintest cluster members will allow us to build on this scenario.

ACKNOWLEDGEMENTS

We thank the referee for constructive comments that helped us to improve the manuscript. This project has been partly supported by the ‘StarFormMapper’ project funded by the European Union’s Horizon 2020 Research and Innovation Action (RIA) programme under grant agreement number 687528. PABG acknowledges financial support from FAPESP (grants: 2013/04934-8 and 2015/14696-2). This research has made use of the computing facilities of the Laboratory of Astroinformatics at IAG/USP (São Paulo, Brazil). This research has also made use of the SIMBAD data base operated at the CDS (Strasbourg, France).

REFERENCES

Adler D. et al., 2017, rgl: 3D Visualization Using OpenGL, Available at <https://CRAN.R-project.org/package=rgl>

Altmann M., Roeser S., Demleitner M., Bastian U., Schilbach E., 2017, *A&A*, 600, L4

Astraatmadja T. L., Bailer-Jones C. A. L., 2016, *ApJ*, 832, 137

Barbier-Brossat M., Figon P., 2000, *A&AS*, 142, 217

Chen C. H., Mamajek E. E., Bitner M. A., Pecaut M., Su K. Y. L., Weinberger A. J., 2011, *ApJ*, 738, 122

Cook N. J., Scholz A., Jayawardhana R., 2017, *AJ*, 154, 256

Dahm S. E., Slesnick C. L., White R. J., 2012, *ApJ*, 745, 56

de Bruijne J. H. J., 1999a, *MNRAS*, 306, 381

de Bruijne J. H. J., 1999b, *MNRAS*, 310, 585

de Zeeuw P. T., Hoogerwerf R., de Bruijne J. H. J., Brown A. G. A., Blaauw A., 1999, *AJ*, 117, 354

Donaldson J., Weinberger A., Gagné J., Boss A., Keiser S., 2017, *ApJ*, 850, 11

ESA ed., 1997, ESA SP-1200: The HIPPARCOS and TYCHO Catalogues. ESA, Noordwijk

Fang Q., Herczeg G. J., Rizzuto A., 2017, *ApJ*, 842, 123

Galli P. A. B., Teixeira R., Ducourant C., Bertout C., Benevides-Soares P., 2012, *A&A*, 538, A23

Galli P. A. B., Moraux E., Bouy H., Bouvier J., Olivares J., Teixeira R., 2017, *A&A*, 598, A48

Girard T. M. et al., 2011, *AJ*, 142, 15

Gontcharov G. A., 2006, *Astron. Lett.*, 32, 759

Holmberg J., Nordström B., Andersen J., 2007, *A&A*, 475, 519

Johnson D. R. H., Soderblom D. R., 1987, *AJ*, 93, 864

Kharchenko N. V., Scholz R.-D., Piskunov A. E., Röser S., Schilbach E., 2007, *Astron. Nachr.*, 328, 889

Kordopatis G. et al., 2013, *AJ*, 146, 134

Lindgren L. et al., 2016, *A&A*, 595, A4

Lodieu N., 2013, *MNRAS*, 431, 3222

Luhman K. L., Mamajek E. E., 2012, *ApJ*, 758, 31

Malo L., Artigau É., Doyon R., Lafrenière D., Albert L., Gagné J., 2014, *ApJ*, 788, 81

Mann A. W. et al., 2016, *AJ*, 152, 61

Nordström B. et al., 2004, *A&A*, 418, 989

Palouš J., Ehlerová S., 2017, in Alsabti A., Murdin P., eds, *Gould’s Belt: Local Large-Scale Structure in the Milky Way, Handbook of Supernovae*. Springer, Cham

Pecaut M. J., Mamajek E. E., 2016, *MNRAS*, 461, 794

Pecaut M. J., Mamajek E. E., Bubar E. J., 2012, *ApJ*, 746, 154

Perrot C. A., Grenier I. A., 2003, *A&A*, 404, 519

Preibisch T., Mamajek E., 2008, in Reipurth B., ed., *ASP Monograph Publications, Handbook of Star Forming Regions, Vol. II: The Southern Sky*. Astron. Soc. Pac., San Francisco, p. 235

Preibisch T., Zinnecker H., 1999, *AJ*, 117, 2381

Preibisch T., Brown A. G. A., Bridges T., Guenther E., Zinnecker H., 2002, *AJ*, 124, 404

R Core Team, 2017, R: A Language and Environment for Statistical Computing. Available at <https://www.R-project.org/>

Rizzuto A. C., Ireland M. J., Robertson J. G., 2011, *MNRAS*, 416, 3108

Rizzuto A. C., Ireland M. J., Kraus A. L., 2015, *MNRAS*, 448, 2737

Rizzuto A. C., Ireland M. J., Dupuy T. J., Kraus A. L., 2016, *ApJ*, 817, 164

Roeser S., Demleitner M., Schilbach E., 2010, *AJ*, 139, 2440

Rousseeuw P. J., Driessen K. V., 1999, *Technometrics*, 41, 212

Rousseeuw P. J., Hubert M., 2011, *Wiley Interdiscip. Rev. Data Min. Knowl. Discov.*, 1, 73

Slesnick C. L., Hillenbrand L. A., Carpenter J. M., 2008, *ApJ*, 688, 377

Song I., Zuckerman B., Bessell M. S., 2012, *AJ*, 144, 8

Torres C. A. O., Quast G. R., da Silva L., de La Reza R., Melo C. H. F., Sterzik M., 2006, *A&A*, 460, 695

Van Aelst S., Rousseeuw P., 2009, *Wiley Interdiscip. Rev. Comput. Stat.*, 1, 71

Venables W. N., Ripley B. D., 2002, *Modern Applied Statistics with S*, 4th edn. Springer, New York. Available at <http://www.stats.ox.ac.uk/pub/MASS4>

Wenger M. et al., 2000, *A&AS*, 143, 9

White R. J., Gabor J. M., Hillenbrand L. A., 2007, *AJ*, 133, 2524

Zacharias N., Finch C. T., Girard T. M., Henden A., Bartlett J. L., Monet D. G., Zacharias M. I., 2013, *AJ*, 145, 44

SUPPORTING INFORMATION

Supplementary data are available at *MNRAS* online.

Please note: Oxford University Press is not responsible for the content or functionality of any supporting materials supplied by the authors. Any queries (other than missing material) should be directed to the corresponding author for the article.

This paper has been typeset from a $\text{\TeX}/\text{\LaTeX}$ file prepared by the author.